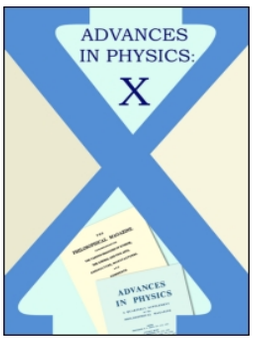

Advances in Physics: X

ISSN: (Print) (Online) Journal homepage: https://www.tandfonline.com/loi/tapx20

Colloidal engines for innovative tests of information thermodynamics

Govind Paneru & Hyuk Kyu Pak

To cite this article: Govind Paneru & Hyuk Kyu Pak (2020) Colloidal engines for innovative tests of information thermodynamics, Advances in Physics: X, 5:1, 1823880, DOI: 10.1080/23746149.2020.1823880

To link to this article: https://doi.org/10.1080/23746149.2020.1823880

Published online: 29 Sep 2020.

ADVANCES IN PHYSICS: X
NULL, VOL. 5, NO. 1, 1823880
https://doi.org/10.1080/23746149.2020.1823880

Taylor & Francis
Taylor & Francis Group

REVIEW

Colloidal engines for innovative tests of information thermodynamics

Govind Paneru[a] and Hyuk Kyu Pak[a,b]

[a]Center for Soft and Living Matter, Institute for Basic Science (IBS), Ulsan, South Korea; [b]Department of Physics, Ulsan National Institute of Science and Technology, Ulsan, South Korea

ABSTRACT

Recent theoretical developments in information thermodynamics elucidated the link between the acquired information and the entropy production through measurement and feedback control by generalizing the fluctuation theorems and the second law of thermodynamics. We summarize here our recent experimental studies based on the colloidal system that have been conducted to test the theoretical findings of information thermodynamics. In particular, we present the design principles of error-free and noisy information engines consisting of a colloidal particle in an optical trap that is capable of performing nearly error-free measurement and ultrafast feedback control. Our perspectives on future experimental studies are also presented.

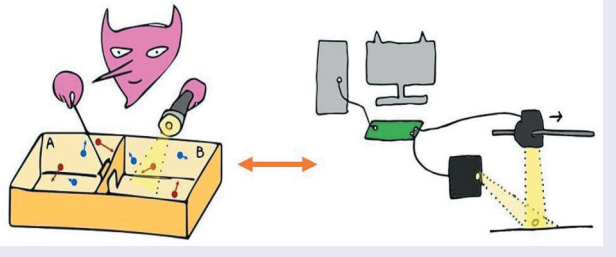

ARTICLE HISTORY
Received 1 June 2020
Accepted 10 September 2020

KEYWORDS
Non-equilibrium thermodynamics; information engines; fluctuation theorems; efficiency fluctuations

Introduction

Understanding the relationship between thermodynamics and information has been a fundamental problem of non-equilibrium physics ever since the paradox of Maxwell's demon [1]. The demon envisioned by Maxwell operates by obtaining the information about the velocities of gas molecules in a box, sorting them into fast and slow ones, thereby decreasing the entropy of the system, resulting in the violation of the second law of thermodynamics (Figure 7A). Resolving this paradox revealed a deep link between the

CONTACT Govind Paneru gpaneru@gmail.com; Hyuk Kyu Pak hyuk.k.pak@gmail.com IBS Center for Soft and Living Matter, Advanced Materials Research Bldg. (#103), Rm.313, Ulsan National Institute of Science and Technology ,50 UNIST-gill, Ulju-gun, Ulsan, 44919, South Korea

information gathered by the demon and thermodynamic entropy of the system [2,3,4,5,6,7], and the field of information thermodynamics has emerged formally after these seminal works. The past decade witnessed significant advances in the field of information thermodynamics that incorporate stochastic thermodynamics [8,9] and fluctuation theorems [10,11,12]. The general theoretical frameworks, which generalizes the fluctuation theorems and the second laws of stochastic thermodynamics for the system in presence of correlation, and information processing such as feedback control and information erasure, were formulated [13–16]. Also, various models for 'Maxwell's demon' type information engines, capable of extracting work from a single heat bath by utilizing information about the microscopic state of the system, were developed [17,18,19,20,21]. Recent technological advances in the active control and precision measurement of small fluctuating systems allowed the experimental realization of information engines in classical systems using colloidal particles [22,23,24,25,26,27,28], a single DNA hairpin [29], a single electron box [30], and a photodetector [31]; and in quantum systems using a superconducting qubit [32]. Consequently, generalized fluctuation theorems and several fundamental principles of information thermodynamics were verified experimentally [22,23,26,32,33,34,35].

Among many examples, colloidal systems, whose dynamics is based on the continuum model of classical Langevin equations, serve as a model system for exploring the field of stochastic and information thermodynamics [8]. Most colloidal information engines studied consist of colloidal particles trapped in a harmonic potential. The operation of these engines is based on the pre-designed feedback control protocol that generally consists of the three steps: measurement of the particle position, the shift of the potential center or the change of the potential stiffness or both, and relaxation [17–19]. Also, the theoretical studies on the colloidal information engines in the presence of external electric and magnetic fields have been reported [36,37]. One of the key features of the colloidal information engine over its discrete electronic counterpart is that its phase space is continuous, such that the mutual information, which measures the correlation between particle position and the measurement outcome, is also continuous. Thus, evaluating mutual information requires measurement of the probability distributions of the particle position and the measurement outcome, which further depends on the error distribution.

The integral fluctuation theorems and their generalizations are generally accepted as the most important discoveries of non-equilibrium physics in the last century. However, they are found not valid for processes with absolute irreversibility, such as free expansion and feedback control with error-free measurements [38,39]. In the case of error-free measurements, the post-measurement state is sharply localized in a narrow region of the

phase space, and the forward path probability vanishes outside this region; while, due to the subsequent feedback control and relaxation, the backward path probability does not vanish, leading to the violation of the generalized integral fluctuation theorem. The fluctuation theorems are generalized recently for the cases of absolute irreversibility and their validity is tested in simple models [38,39].

The main focus of this review is to present the latest advances in the design of classical information engines that consists of a colloidal particle in a harmonic trap generated by optical tweezers. Optical tweezers have been used extensively in the past for realizing two temperature bath stochastic heat engines and verification of fluctuation theorems [8,40,41]. For the case of information engines, Toyabe et al. [22] designed the first discrete state error-free engine consisting of a colloidal particle in spiral-staircase-like potential and demonstrated the work extraction from a single heat bath using Shannon information. Such discrete state colloidal information engines have been reviewed previously [13,14]. Although these studies succeeded in realizing the thought experiments such as Maxwell's demon and Szilard's engine, there was still a lack of experiments for realizing the theoretically proposed continuous state noisy information engines involving an error in the measurement and feedback control [17,42,43]. Noisy information engines are widespread in nature, particularly in biological systems where signal transduction and perception occur in noisy environment [44–47]. Thus, complementing these previous reviews, we summarize our recent experimental

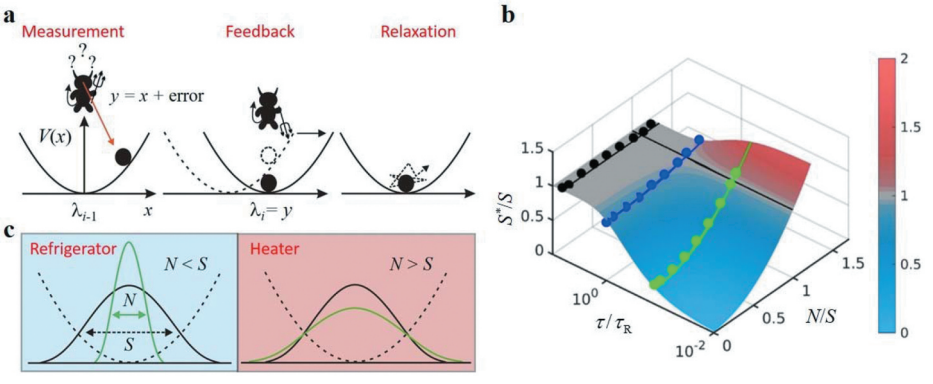

Figure 1. a Illustration of the *i*-th engine cycle. b Contour plot of the normalized steady state variance S^*/S of the probability distribution of the particle position in steady state as a function of noise level *N*/S and cycle period τ/τ_R. The solid circles are the plot of experimentally obtained values of S^*/S as a function of N/S when τ is 0.5 (green circles), 3 (blue) and 20 (black) ms. The solid curves are from the model. The black line parallel to τ/τ_R axis denotes $N/S = 1$ and separates the refrigerator (blue) and heater (red) region of the engine. **c** Illustration of the noise-induced cooling and heating regimes. The system works as a refrigerator (heater) when $N < S$ ($N > S$), where S is the variance of the equilibrium distribution (solid black) and N is the variance of the noise distribution (solid green). Figures adapted from Ref [26].

findings on error-free and noisy information engine, consisting of a colloidal particle in an optical trap [23–26,48]. By combining high-precision position detection and ultrafast feedback control, our set up can directly measure, control, and vary the error level and hence the mutual information passing through the feedback loop. In addition to the first test of the generalized integral fluctuation theorems, we present the design principles optimized for maximum work and power extraction, as well as the information conversion efficiency and the systematic studies of the efficiency fluctuations over the entire non-equilibrium phase space of the engine. For example, our lossless information engine converts nearly all available information into work through error-free measurements, achieving the equality of the generalized second law for the case of absolute irreversibility [23]. We also show the information processing and asymmetric feedback rectify the directed motion. Apart from ours, the recent experimental works on information engines consisting of a colloidal particle attached to the DNA hairpin [29] and a colloidal particle under the flow field [28] are also significant.

The mutual information fueled colloidal engine

The mutual information engine consists of a 2μm diameter colloidal particle diffusing within the harmonic potential $V(x,t) = (k/2)(x-\lambda(t))^2$ of an optical trap in a bath of temperature $V(x,t) = (k/2)(x-\lambda(t))^2$(Figure 1A). The details of the optical trap set up with real-time feedback control can be found in Refs. [23,24,26] and are briefly described in Methods and Figure 7B. Here, x is the position of the particle at the time$t$, k is the trap stiffness, and $\lambda(t)$ is the center of the trap. In the absence of feedback, the particle position follows the equilibrium Gaussian distribution of zero mean and variance $\lambda(t)$. Note that our system can measure the particle position x precisely at a resolution of 1 nm. So, in comparison to the particle fluctuation $\sqrt{S} \approx 28$nm, the error in x is negligible. The trap stiffness is calibrated as $k = k_B\, T/S,$ The characteristic relaxation time of the particle in the harmonic trap is $\tau_{\mathrm{R}} = \gamma/k \approx$ 3.5ms, where γ is the Stokes friction coefficient.

Each engine cycle of duration τ includes three processes: measurement of the particle position, the shift of the trap center, and relaxation (Figure 1A). The ith engine cycle operates with practically instantaneous and nearly error-free detection of the particle position x with respect to the trap center λ_{i-1}. A numerically generated Gaussian noise, $p(y|x) = \sqrt{1/2\pi N}\exp[-(y-x)^2/2N]$, of variance N (greater than the measurement error, $\sqrt{N} > 1$nm) is added to x as an error, and the feedback loop observes this distorted value, $y = x +$ error, as the particle position [26]. The trap center is then shifted instantaneously to y. This is followed by a relaxation step

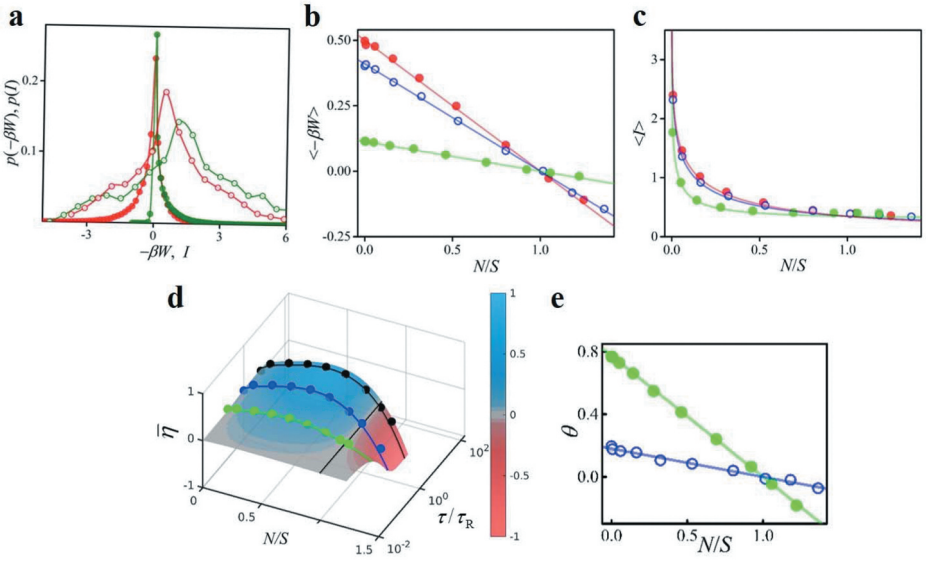

Figure 2. **a** Plot of probability distribution functions of mutual information I (open circles) and extracted work $-\beta W$ (filled circles) for cycle period $\tau = 3$ms and error-level N/S of 0.06 (olive) and 0.53 (red). The solid curves are guides to the eyes. **b** The average extracted work $\langle -\beta W \rangle$ as a function of noise level N/S, for $\tau = 20$ (red circles), 3 (blue) and 0.5 (green) ms. **c** The measured average mutual information in steady state $\langle I \rangle$, as a function of N/S for $\tau = 20$ (red circles), 3 (blue) and 0.5 (green) ms. **d** The information utilization efficiency, $\bar{\eta} = \langle -\beta W \rangle / \langle I \rangle$, as a function of N/S and τ/τ_R. Solid circles are experimentally obtained $\bar{\eta}$ for $\tau = 20$ (black circles), 3 (blue) and 0.5 (green) ms. **e** The "cooling efficiency", $\theta = 1 - T_{\text{eff}}/T$, as a function of error N/S for $\tau = 0.5$ (green circles) and 3 (blue) ms. The solid curves are fit to the model. a-e adapted from Ref. [26].

that lasts for a period τ. In the subsequent $(i+1)$th cycle, the particle position is measured with respect to the shifted potential center λ_i (the origin is reset), and the same protocol is repeated. Since the origin is reset, the process does not depend on all previous measurements. After many repetitions of the measurement-feedback-relaxation cycles, the engine reaches a steady state. The steady-state probability distributions of the particle position $p(x)$ after the relaxation (at the beginning of each cycle) is also Gaussian with zero mean but of different variance, $S^* = S + (N - S)e^{-2\tau/\tau_R}$. We show that the variance of the distribution can narrow or widen depending on the noise level, N/S, consequently, the effective temperature of the particle is $k_B T_{\text{eff}} = kS^*$ (Figure 1B). Thus, the information engines perform as refrigerators ($T_{\text{eff}}/T = S^*/S < 1$) for $N < S$, or as heaters ($T_{\text{eff}}/T > 1$) for $N > S$, as shown in Figure 1C. Prior research works used feedback control to cool the system [49], and noise to heat the system [50]. The noisy information engine presented here demonstrates both, the effective cooling and the heating, which is solely controlled by the noise level.

Measurement of thermodynamic quantities

Work

We measure the energetics of the engine during the measurement-feedback-relaxation cycle. The measurement process neither changes the microstate nor the potential energy of the particle; therefore, no work is performed on the particle during the measurement step. The work performed on the particle during the feedback step (when the trap center is instantaneously shifted) is equal to the change in the potential energy of the particle. Since the trap center remains fixed, no work is performed on the particle during the relaxation step, and only heat is dissipated. Thus, the work performed on the particle per cycle is $\beta W \equiv \beta \Delta V = (1/2)\beta k[(x-y)^2 - x^2]$. The average work performed on the particle per cycle in steady-state is

$$\langle \beta W \rangle = \frac{1}{2}\beta k \int dx\, dy\, p(x|y)p(y)\left[(x-y)^2 - x^2\right] = -\frac{1}{2}\left(\frac{S^* - N}{S}\right), \qquad (1)$$

where $p(x|y)$is the conditional probability distribution of the particle position $x$immediately after the measurement and $p(y)$ is the distribution of the measurement outcome y [26]. The distribution of the extracted work $-\beta W$ in steady-state conditions for several regimes of engine accuracy is shown in Figure 2A. Error-free engines ($N = 0$) always extract positive work. On the other hand, noisy engines ($N > 0$) often make mistakes in their feedback and have a non-zero probability for negative work extraction. Engines with relatively small noise level ($N/S < 1$), on an average, always extract positive work from, $\langle -\beta W \rangle > 0$, performing as refrigerators. At the other extreme, the average work extracted from the engines with $N/S > 1$ is always negative, $\langle -\beta W \rangle < 0$, performing as heaters. In this regard, the average work extracted from the marginal engines ($N/S = 1$) is zero. The average extracted work decreases for faster ($\tau < \tau_R$) and noisy engines ($N > 0$) (Figure 2B). The maximal average work $\langle -\beta W \rangle = 0.498 \pm 0.003$, is extracted by perfect engines whose cycle is long enough to reach equilibrium, in agreement with the theoretical value 0.5 (Eq. (1)). While the ultrafast engines ($\tau \to 0$) do not extract work, $\langle -\beta W \rangle \to 0$, they extract maximum average power $P \equiv \langle -\beta W \rangle / \tau \to (1 - N/S)/\tau_R$.

Mutual information

We demonstrated the quantification of the mutual information, between the particle position x and the measurement outcome y, for continuous engines. The mutual information gain by the feedback loop at the time of measurement is given by $I = \ln[p(x|y)/p(x)]$. The average mutual information gain in steady-state is then given by

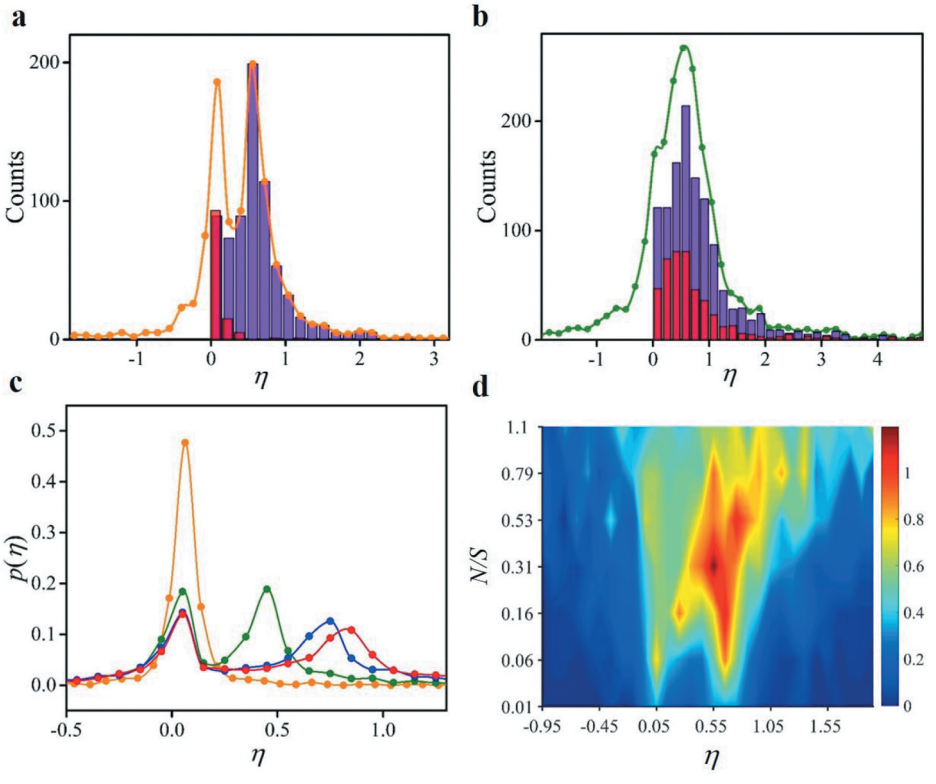

Figure 3. Measurement of efficiency fluctuations. **a, b** Histograms of the experimentally measured efficiency $\eta = -\beta W/I$ for $\tau = 3$ ms and $N/S = 0.06$ (orange), and 0.32 (olive). The solid curves are guides to the eyes. The violet (red) bars correspond to $\beta W < 0$ ($\beta W > 0$) and $I > 0$ ($I < 0$), respectively. **c** Efficiency distribution (from simulation) for $N/S = 0.034$ at four different cycle times $\tau = 0.1$ (orange), 1 (olive), 3 (blue), and 10 (red) ms. **d** Contour plot showing the fluctuations in efficiency distribution as a function of noise level N/S for $\tau = 3$ ms. Figures adapted from Ref. [26].

$$\langle I \rangle = \int dx\, dy\, p(x|y)p(y) \ln \frac{p(x|y)}{p(x)} = \frac{1}{2} \ln \left(1 + \frac{S^*}{N} \right). \tag{2}$$

Some amount of this information gain is utilized for work extraction during the feedback step. The remaining information is erased by resetting the trap center at the end of each relaxation step. Thus, the average information gain per cycle is $\langle \Delta I \rangle = \langle I \rangle$. Figure 2A shows the distribution of mutual information I. The interesting feature of this plot is that I fluctuates and takes both positive and negative values; however, its average is always positive, $\langle I \rangle \geq 0$. Also, the peak of $p(I)$ shifts towards zero with an increase in the noise level owing to the sharp decrease in I. The measured $\langle I \rangle$ is smaller for larger noise level N or shorter cycles τ, (Figure 2C). However, it always remains greater than the average extracted work, $\langle -\beta W \rangle \leq \langle I \rangle$. Noting that there is no free energy change per cycle in steady-state, $\Delta F =$

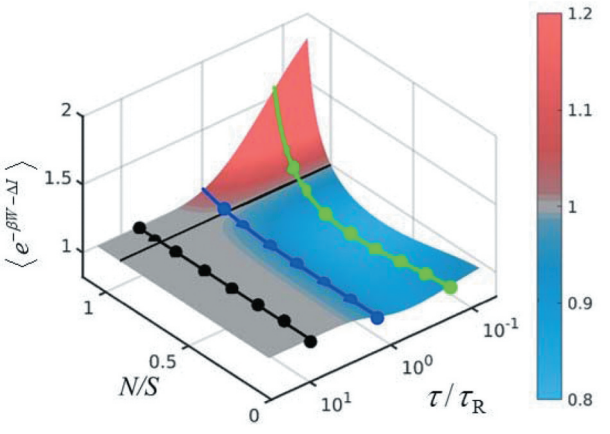

Figure 4. Contour plot of $\langle \exp(-\beta W - \Delta I)\rangle$ as a function of *N*/S and τ/τ_R. The solid circles are the experimental plot of $\langle \exp(-\beta W - \Delta I)\rangle$ as a function of *N*/S for $\tau = 20$ (black circles), 3 (blue circles), and 0.5 (green circles) ms. The solid curves are theoretical results (adapted from Ref. [26]).

0, the feedback protocol always satisfies the second law of information thermodynamics, $\langle -\beta W\rangle \leq -\beta\Delta F + \langle \Delta I\rangle$ [42]. The information gained by perfect engines ($N = 0$) diverges.

Efficiency

We also measured the average information conversion efficiency, $\bar{\eta} \equiv \langle -\beta W\rangle / \langle I\rangle$, and found that the most efficient engines are relatively noisy ones (Figure 2D). The global maximum $\bar{\eta} \approx 0.48$ is obtained for a slower engine ($\tau > > \tau_R$) at a finite noise level $N/S \approx 0.36$. This efficiency is larger than the discrete-state colloidal information engine realized in Ref [22]. Also, our observation of maximum efficiency at a finite noise level cannot be predicted from a recently demonstrated discrete information engine [32], which shows efficiency maximum at $N/S \to 0$. The engines with $N/S > 1$ exhibit negative efficiency since extracted work is negative, $\langle -\beta W\rangle < 0$.

One may also define a 'cooling efficiency', $\theta \equiv 1 - T_{eff}/T$, akin to the Carnot efficiency of conventional heat engines (Figure 2E). As expected, lowering the noise level *N*/*S* and shortening the period τ increase the cooling efficiency θ. Such engines produce a very sharp steady-state distribution since the particle can hardly move before the next cycle begins. The ultrafast and perfect engines ($N = 0$, $\tau \to 0$) shrink the distribution into a delta function, equivalent to zero effective temperature, $T_{\text{eff}} = 0$, and maximal cooling efficiency, $\theta = 1$ is achieved. The negative θ for $N/S > 1$ refers to the effective heating. The effective heating increases with increasing the noise level and shortening the cycle period.

Efficiency fluctuations

Recent studies demonstrated that the stochastic efficiency of Brownian heat engines driven by the non-equilibrium protocol is not bounded and can even exceed Carnot efficiency [51–58]. Here, we study the stochastic efficiency $\eta \equiv -\beta W/I$ of the information engine owing to the fluctuations in work and mutual information (Figure 3). The efficiency distribution exhibits double peaks for smaller noise level (Figure 3A), that coalesce into a single peak at the noise level for which $\bar{\eta}$ is maximal (Figure 3B). For higher noise levels, $p(\eta)$ broadens and its peak shifts towards $\eta = 1$. The observed double peaks of the efficiency distribution $p(\eta)$ are the outcome of an interplay between the distributions of extracted work $p(-\beta W)$ and mutual information $p(I)$ (Figure 2A): At low noise level, the peaks of $p(-\beta W)$ and $p(I)$ are well separated, giving rise to double peaks. At a higher error level, they get closer, owing to a sharp decrease in I, and the peaks coalesce.

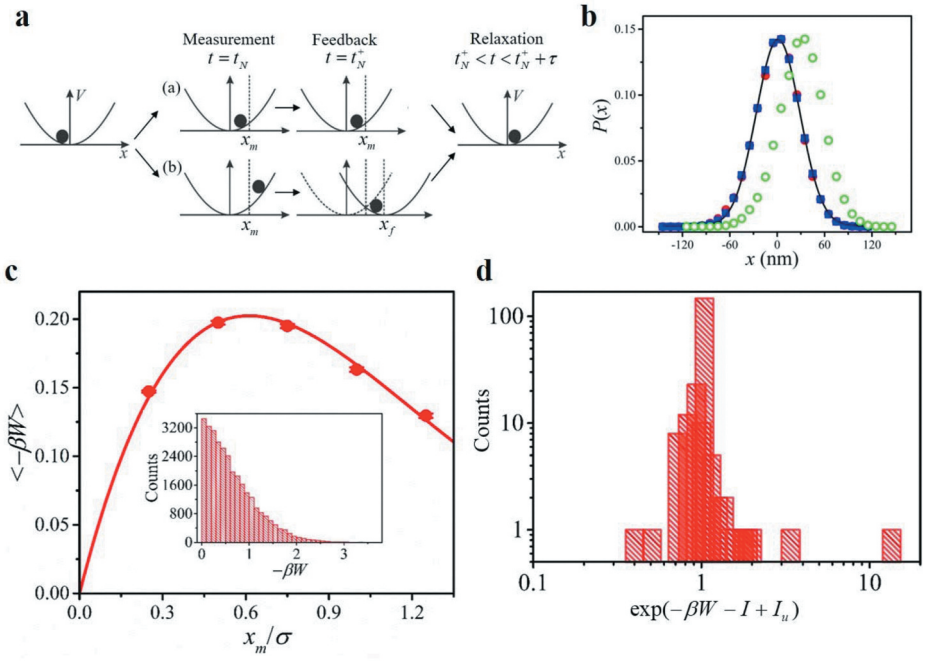

Figure 5. **a** Illustration of the N th feedback cycle (adapted from Ref. [24].). **b** Probability distribution $P(x)$ of the particle position in thermal equilibrium (red solid circles), and measured every 25 ms during each engine cycle (blue solid squares) for $x_m = 0.5\sigma$. The shifted probability distribution $P(x - 2x_m)$ is obtained by performing the backward protocol (green open circles). The black solid curve is a fit to the Boltzmann distribution, $P(x) = (2\pi\sigma^2)^{-1/2} \exp[-x^2/(2\sigma^2)]$. **c** Average extracted work as a function of x_m/σ. The solid curve is a theoretical result. Inset: Histogram of the extracted work $-\beta W$ for $x_m = 0.5\sigma$. **d** Distribution of $\exp(-\beta W - I + I_u)$ in order to verify the generalized Jarzynski equality in Eq. (4). b-d adapted from Ref. [23].

We also show that the observed peaks are mainly due to the negative values of βW for which I is positive (purple bars). Nevertheless, there is also a significant contribution from positive βW for which $I$is negative (red bars), especially for large noise levels, resulting in a maximal average efficiency at a finite noise level. In comparison to the recent theoretical work [59], the observed peaks in the efficiency distribution $p(\eta)$ of the information engine are mainly due to $\beta W < 0$ and $I > 0$. Also, we do not observe a minimum near $\eta = 1$, and the tail part of $p(\eta)$ does not follow the universal power-law $p(\eta \to \pm\infty) \sim \eta^{-2}$ [59–61]. The global maximum of $p(\eta)$is found near $N/S \approx 0.32$(Figure 3D), at which the average efficiency, $\bar{\eta} = \langle -\beta W \rangle / \langle I \rangle$ is also maximal.

Test of integral fluctuation theorem

The integral fluctuation theorem for the feedback-controlled systems has the following form [13,42]

$$\left\langle e^{-\beta(W-\Delta F)-\Delta I} \right\rangle = 1. \tag{3}$$

It has been known that this theorem works only for the system under measurement and feedback control whose initial or final states are in equilibrium. We test the integral fluctuation theorem in Eq. (3) and check how far the average deviates from unity for our cyclic information engine with non-equilibrium initial and final states (Figure 4). We find that $\langle e^{-\beta W-\Delta I} \rangle = 1$ regardless of error size for $\tau >> \tau_R$ (black circles), for which the engine is fully relaxed at the end of each cycle. Another interesting observation is that $\langle e^{-\beta W-\Delta I} \rangle = 1$when $N = S$ regardless of the cycle period. For finite τ,$\langle e^{-\beta W-\Delta I} \rangle$ deviates from unity, even nearτ_R for which the system reaches near equilibrium (blue circles). Interestingly, $\langle e^{-\beta W-\Delta I} \rangle$ is found to be always less (greater) than one in the cooling (heating) region of the engine.

Information thermodynamics with absolute irreversibility: system under error-free measurements and feedback control

For error-free measurement, the information gain is given by the Shannon information. In this case, the generalized integral fluctuation theorem in Eq. (3) has been generalized by subtracting unavailable information I_u from the Shannon information gain I [39],

$$\langle \exp[-\beta(W - \Delta F) - (I - I_u)] \rangle = 1. \tag{4}$$

Applying Jensen's inequality to Eq. (4) yields a generalized second law [39],

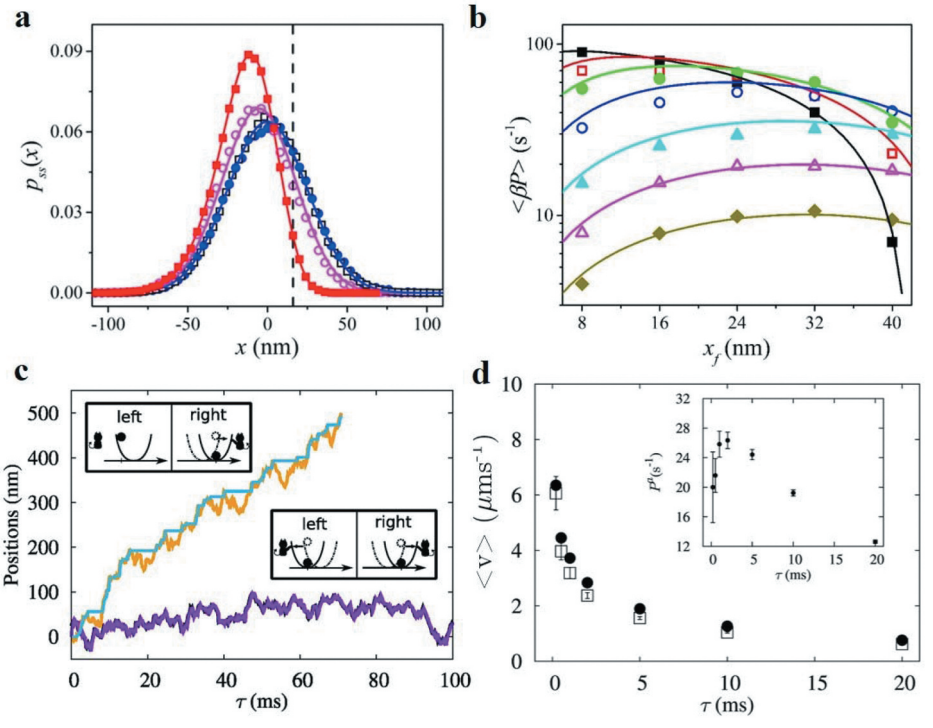

Figure 6. **a** Steady-state probability distribution of the particle position for different τ with x_m = 16 nm and x_f = 32 nm. The red solid squares, magenta open circles, and blue solid circles correspond to τ = 0.2, 2.0, and 20.0 ms, respectively. The distribution measured for τ = 20 ms follows the equilibrium distribution obtained without feedback control (see black open squares). The solid curves represent the analytical results. The dashed vertical line corresponds to $x_m = 16$nm. **b** Average extracted power as a function of x_f for different τ with x_m fixed at 16 nm. The black solid squares, red open squares, green solid circles, blue open circles, cyan solid triangles, magenta open triangles and dark yellow solid diamonds correspond to the average power for τ = 0.2, 0.5, 1.0, 2.0, 5.0, 10.0, and 20.0 ms, respectively. The solid curves are the plots of $\langle -\beta W \rangle_{ss}/\tau$. **c** Particle trajectories for symmetric and asymmetric feedback control. For symmetric feedback (lower inset), particle position x is measured and trap center λ is shifted to the measured outcome, $\lambda = x$. The resulting trajectories for x (black) and λ (magenta) show random distribution. For asymmetric feedback (upper inset), the trap center is shifted to the measurement outcome $x$only when $x \geq 0$. The resulting trajectories for x (orange) and λ (blue) are driven in the positive direction. **d** Plot of average transport velocity as a function of cycle period τ. Open squares correspond to the velocity induced by the asymmetric cooling and closed circles correspond to the upper bound for the velocity. The error bars denote the standard error of the mean. Inset: Extracted power as function of τ. a-b adapted from Ref [24]. and c-d from Ref [25].

$$\langle -\beta W \rangle \leq -\beta \Delta F + \langle I \rangle - \langle I_u \rangle. \tag{5}$$

Namely, the work extracted from the information engine $\langle -\beta W \rangle$ cannot exceed the sum of the free energy difference between the final and initial states $-\beta \Delta F$ and the available information $\langle I \rangle - \langle I_u \rangle$.

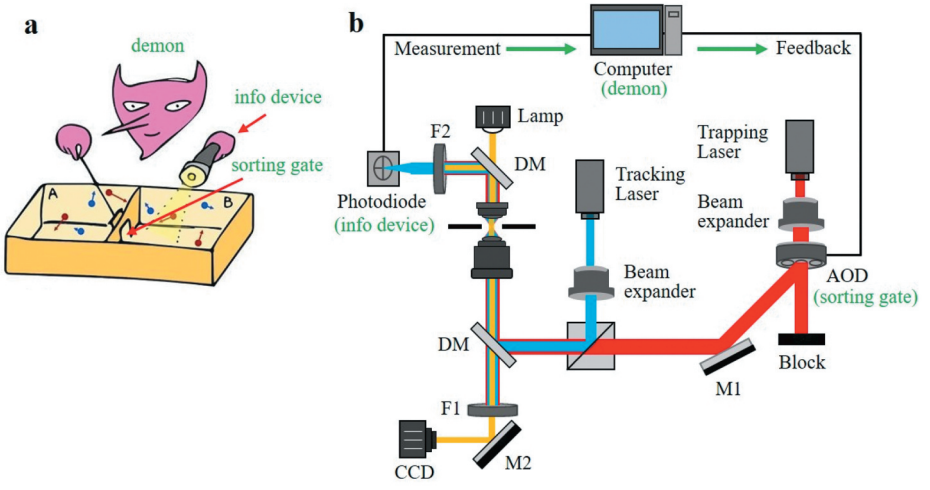

Figure 7. Comparison of Maxwell's demon with colloidal engine setup. **a** Schematic of Maxwell's demon. By measuring the velocities of the gas molecules and opening and closing the gate, the demon can sort the hotter ones (red) in the left half of the box, and the colder ones (blue) in the right half, creating the temperature difference. **b** Schematics of the modern Maxwell demon consisting of the colloidal particle in the optical trap subjected to the real-time measurement and feedback control. Here, computer, photodiode, and AOD play the role of the demon, info device, and sorting gate, respectively (adapted from Ref [26].)

In this section, we discuss the first realization of error-free colloidal engines that tests the integral fluctuation theorem in Eq. (4) and achieves the tight bound of Eq. (5) [23]. Figure 5A shows the corresponding feedback protocol. We set a reference line at x_m and perform a nearly error-free measurement (with the resolution of 1 nm) of the particle position to determine which side of the reference line the particle is located at. If the particle is found on the left of x_m, we do nothing. Whereas, if the particle is found on the right of x_m, the potential center is instantaneously shifted to a new position x_f. After the feedback step, the system is allowed to relax for a time τ. Repeating the measurement-feedback-relaxation cycle, the engine can transport the particle, thereby extracting work from the random thermal fluctuations of the surrounding heat bath. Each engine cycle is characterized by three parameters: the setting distance x_m, the potential center moving distance x_f, and the periodτ for relaxation. The optimal operating condition depends on the choice of these parameters.

The trap stiffness is calibrated by fitting the probability distribution of the particle position in thermal equilibrium without the feedback process to the Boltzmann distribution $P(x) = (2\pi\sigma^2)^{-1/2} \exp[-x^2/(2\sigma^2)]$. In Figure 5B the standard deviation is $\sigma = 28$nm. We set $x_m = 0.5\sigma = 14$nm and $x_f = 2x_m$, and operate the engine for $\tau >> \tau_R$ such that the particle is fully relaxed after feedback. The distribution (blue squares in Figure 5B), which is obtained from

100,000 feedback cycles, is indistinguishable from the equilibrium distribution (red). The inset of Figure 5C shows the distribution of the measured extracted work per cycle, $-\beta W(x) = \beta[V(x) - V(x-2x)]$ for $x \geq x_m$ and $-\beta W(x) = 0$ for $x \leq x_m$, whose average is $\langle -\beta W_{\text{exp}} \rangle = 0.197 \pm 0.001$.

Theoretically, the average extracted work per cycle is given by

$$\langle -\beta W \rangle = -\int_{-\infty}^{\infty} dx\, P(x)\beta W(x) = 2\pi^{-1/2}\ell e^{-\ell^2} - 2\ell^2 \text{erfc}(\ell), \tag{6}$$

where $\ell = 2^{-1/2}(x_m/\sigma)$ and $\text{erfc}(z) = 2\pi^{-1/2}\int_z^{\infty} e^{-t^2} dt$ is the complementary error function. The value of the average extractable work obtained from the theoretical model, $\langle -\beta W_{\text{model}} \rangle = 0.198 \pm 0.002$, agrees well with the experimental value.

For error-free measurement, the average information gain at the time of measurement is given by Shannon information [39],

$$\langle I \rangle = -\lim_{\Delta \to 0} \int_{-\infty}^{\infty} dx\, P(x) \ln[P(x)\Delta] = \lim_{\Delta \to 0} \ln \sqrt{2\pi e(\sigma/\Delta)^2}, \tag{7}$$

where the limit of vanishing measurement error $\Delta \to 0$ ensures the positive-definiteness of the entropy and the correspondence between discrete and differential entropies. Some part of this information becomes unavailable during the relaxation phase of the feedback process. The unavailable information $\langle I_u \rangle$ is calculated from the backward process,

$$\begin{aligned} \langle I_u \rangle &= -\lim_{\Delta \to 0} \left\{ \int_{-\infty}^{x_m} dx P(x) \ln[P(x)\Delta] + \int_{x_m}^{\infty} dx P(x) \ln[P(x-2x_m)\Delta] \right\} \\ &= -2\pi^{-1/2}\ell e^{-\ell^2} + 2\ell^2 \text{erfc}(\ell) + \lim_{\Delta \to 0} \ln \sqrt{2\pi e(\sigma/\Delta)^2}. \end{aligned} \tag{8}$$

Using the equilibrium probability distribution $P(x)$and the shifted one $P(x-2x_m)$ from Figure 5B, we measure the net available information $\langle I \rangle - \langle I_u \rangle = 0.200 \pm 0.002$, which is close to the measured extracted work. This demonstrates the sharpness of the bound set by the generalized second law in Eq. (5). To find the optimal feedback protocol, we evaluate the extracted work as a function of x_m/σ (Figure 5C). The maximum of average extracted work is obtained at $x_m \approx 0.6\sigma$. Finally, we demonstrate the generalized integral fluctuation theorem in Eq. (4) is satisfied with the feedback protocol (see Figure 5D). To this end, we evaluate the value of $\langle \exp[-\beta(W - \Delta F) - (I - I_u)] \rangle$ and found it to be equal to 1.02 ± 0.06.

Optimal tuning of the information engine

We also conduct the parametric study of the error-free information engine operating in non-equilibrium steady states to find the condition for

maximum work, power, and efficiency [24]. We find that the optimal value of x_m for maximum work extraction is near $x_m \sim 0.6\sigma$ (Figure 5C). In the following study, we fix $x_m \sim 0.6\sigma$ and vary x_f and τ to find the optimal condition for maximum work and power extraction. For faster engines ($\tau << \tau_R$), the probability distribution of the particle position in a steady state $p_{ss}(x)$ is a highly asymmetric function (Figure 6A). It spreads out to the right of x_m on increasing τ and matches the equilibrium distribution for $\tau \gtrsim 5\tau_R$. Figure 6B shows the plot of experimentally measured average extracted power $\langle \beta P \rangle = \langle -\beta W \rangle / \tau$ as a function of τ and x_f, respectively, when x_m is fixed at 16 nm. The global maximum of average-extracted work $\langle -\beta W_{\text{model}} \rangle = 0.198 \pm 0.002$ is obtained when $x_f = 2x_m$ and $\tau \gtrsim 5\tau_R$. On the other hand, the global maximum of $\langle \beta P \rangle$ is obtained when $\tau << \tau_R$ and $x_f << x_m$. This is in agreement with the recent theoretically realized Brownian information engine [19], which shows that the extracted power is maximum when $\tau \to 0$ and $x_f \to 0$. However, for $x_f \geq x_m$, $\langle \beta P \rangle$ is found to be maximum for $\tau \sim \tau_R$. The asymmetric feedback control enhances the directed motion of the particle and hence its transport velocity (Figure 6C) [25]. We measured the transport velocity of the information-driven Brownian motor with nearly error-free measurement and asymmetric feedback control. The average transport velocity per cycle increases for faster engines ($\tau << \tau_R$) and gets saturated to zero for slower engines ($\tau \gtrsim 5\tau_R$) (Figure 6D). It is bounded by $\langle v \rangle \leq \sqrt{2N\langle P \rangle / k\tau}$, where $N = \int_{x_m}^{\infty} p_{ss}(x)dx$ is the probability of finding the particle on the right of x_m.

Discussion

We presented here a review of the recent experimental aspects of information thermodynamics for classical systems using colloidal information engines. Information engines are a special class of feedback control systems that extract work from the information about the microstate of the system. As a result, in contrast to standard thermodynamic forces, the feedback systems do not affect the first law of thermodynamics but only affect the balance in the second law. In particular, the measurement initiates the correlation between the entropies of the system and the detector via mutual information. The second law and the fluctuation theorems are generalized by incorporating mutual information in the total entropy. By directly controlling and measuring the mutual information passing through the noisy detector, the colloidal information engines discussed here fully characterized the information-energy interplay over a wide variety of non-equilibrium steady states and verified the generalized second law and integral fluctuation theorems.

The more general fluctuation theorems valid for systems under arbitrary measurement and feedback control, such as the fluctuation theorems for total entropy production [62], or the generalized detailed fluctuation theorems [15], which require the measurement of the heat, entropy, and mutual information along individual forward and backward trajectories, are yet to be verified experimentally.

Most studies in information thermodynamics mainly focus on resolving the paradox imposed by Maxwell's demon, where entropy production and mutual information between the system and the demon are treated on an equal footing. Unlike the above example, the interacting physical systems exchange both energy and information [63]. Also, the signal transduction in the living system occurs in a noisy environment. To understand the mechanism, signal transduction has been modeled as noisy information processing where information flow in the noisy environment plays a significant role [46,47]. The application of information thermodynamics in interacting systems, especially in biological systems is an active emerging field, with a huge scope for experimental studies.

The information engines realized so far require an external control system such as computers and relevant switching devices. Such non-autonomous engines consume more energy than the work they produce. There are reports on the design of autonomously operating Maxwell's demon type stochastic engines, where feedback operation takes place internally [20,64]. Also, autonomous Maxwell's demons consisting of electronic and mechanical devices have been realized experimentally [65,66]. However, the realization of the self-directed colloidal engines is still challenging. It will open new direction and lead to the development of synthetic micro-motors which can convert thermal fluctuations into mechanical work mimicking the real biological motors.

Methods

Experimental setup

The details of the experimental setup are described in our recently published works [23,24,26]. Briefly, a laser with 1064 nm wavelength is used for trapping the particle. The laser Figure 7. Comparison of Maxwell's demon with colloidal engine setup. **a** Schematic of Maxwell's demon. By measuring the velocities of the gas molecules and opening and closing the gate, the demon can sort the hotter ones (red) in the left half of the box, and the colder ones (blue) in the right half, creating the temperature difference. **b** Schematics of the modern Maxwell demon consisting of the colloidal particle in the optical trap subjected to the real-time measurement and feedback control. Here,

computer, photodiode, and AOD play the role of the demon, info device, and sorting gate, respectively (adapted from Ref [26].) is fed to an acoustic optical deflector (AOD). The AOD is controlled via an analog voltage-controlled radio-frequency (RF) synthesizer driver. A second laser with 980 nm wavelength is used for tracking the particle position. A quadrant photodiode (QPD) is used to detect the particle position. The electrical signal from QPD is amplified by a current-to-voltage amplifier and sampled at every$\tau$with a field-programmable gate array (FPGA) data acquisition board. The QPD can measure the particle position at 1 nm resolution. The sample cell consists of a highly diluted solution of 2.0 μm diameter polystyrene particles suspended in deionized water. All experiments were carried out at 293 ± 0.1 K.

Feedback control design

The FPGA board controlled by the LabVIEW software generates the bias voltage that corresponds to the initial position of the trap center to which a particle is trapped. This bias voltage is applied to the AOD via RF synthesizer. The QPD measures the position x of the particle with high accuracy of 1 nm. A Gaussian error of variance N is added to x to get the measurement outcome $y = x +$ error. To shift the trap center to the measurement outcome y, the FPGA board generates an updated bias voltage. After shifting the trap center, we wait for timeτ, during which the particle relaxes in the updated trap center, and another cycle is repeated. The decision of whether to update the bias voltage and shift the potential center is taken in ~20 μs.

Acknowledgments

We would like to acknowledge all collaborators involved in the research. We thank Sandipan Dutta and Tsvi Tlusty for valuable suggestions and thank Burdette Choi for the artistic image of Maxwell's demon. This work was supported by the Institute of Basic Science, South Korea grant no. IBS-R020-D1.

Disclosure statement

No potential conflict of interest was reported by the authors.

Funding

This work was supported by the South Korean Institute for Basic Science, project code IBS-R020-D1.

References

[1] Leff HS, Rex AF. Maxwell's Demon 2: entropy, classical and quantum information, computing. New Jersey: Princeton University Press; 2003.
[2] Szilard L. Über die Entropieverminderung in einem thermodynamischen System bei Eingriffen intelligenter Wesen. Zeitschrift für Physik. 1929;53:840.
[3] Brillouin L. J Appl Phys. 1951;22:334-337.
[4] Landauer R. Irreversibility and heat generation in the computing process. IBM J Res Dev. 1961;5:183.
[5] Bennett CH. The thermodynamics of computation—a review. Int J Theor Phys. 1982;21:905.
[6] Maruyama K, Nori F, Vedral V. Colloquium: the physics of Maxwell's demon and information. Rev Mod Phys. 2009;81:1.
[7] Sagawa T, Ueda M. Minimal energy cost for thermodynamic information processing: measurement and information erasure. Phys Rev Lett. 2009;102:250602.
[8] Seifert U. Stochastic thermodynamics, fluctuation theorems and molecular machines. Rep Prog Phys. 2012;75:126001.
[9] Van den Broeck C, Esposito M. Ensemble and trajectory thermodynamics: a brief introduction. Phys A Stat Mech Appli. 2015;418:6.
[10] Gallavotti G, Cohen EGD. Dynamical ensembles in nonequilibrium statistical mechanics. Phys Rev Lett. 1995;74:2694.
[11] Jarzynski C. Nonequilibrium equality for free energy differences. Phys Rev Lett. 1997;78:2690.
[12] Crooks GE. Entropy production fluctuation theorem and the nonequilibrium work relation for free energy differences. Phys Rev E. 1999;60:2721.
[13] Parrondo JMR, Horowitz JM, Sagawa T. Thermodynamics of information. Nat Phys. 2015;11:131.
[14] Ciliberto S. Experiments in stochastic thermodynamics: short history and perspectives. Phys Rev X. 2017;7:021051.
[15] Potts PP, Samuelsson P. Detailed fluctuation relation for arbitrary measurement and feedback schemes. Phys Rev Lett. 2018;121:210603.
[16] Still S. Thermodynamic cost and benefit of memory. Phys Rev Lett. 2020;124:050601.
[17] Abreu D, Seifert U. Extracting work from a single heat bath through feedback. EPL (Europhysics Letters). 2011;94:10001.
[18] Bauer M, Abreu D, Seifert U. J Phys a-Math Theor. 2012;45:162001 (8pp).
[19] Park J-M, Lee JS, Noh JD. Optimal tuning of a confined Brownian information engine. Phys Rev E. 2016;93:032146.
[20] Mandal D, Jarzynski C. Work and information processing in a solvable model of Maxwell's demon. Proc Nat Acad Sci. 2012;109:11641.
[21] McGrath T, Jones NS, Ten Wolde PR, et al. Biochemical machines for the interconversion of mutual information and work. Phys Rev Lett. 2017;118:028101.
[22] Toyabe S, Sagawa T, Ueda M, et al. Experimental demonstration of information-to-energy conversion and validation of the generalized Jarzynski equality. Nat Phys. 2010;6:988.
[23] Paneru G, Lee DY, Tlusty T, et al. Lossless Brownian Information Engine. Phys Rev Lett. 2018;120:020601.
[24] Paneru G, Lee DY, Park J-M, et al. Optimal tuning of a Brownian information engine operating in a nonequilibrium steady state. Phys Rev E. 2018;98:052119.

[25] Lee DY, Um J, Paneru G, et al. An experimentally-achieved information-driven Brownian motor shows maximum power at the relaxation time. Sci Rep-Uk. 2018;8:12121.
[26] Paneru G, Dutta S, Sagawa T, et al. Efficiency fluctuations and noise induced refrigerator-to-heater transition in information engines. Nat Commun. 2020;11:1012.
[27] Lopez BJ, Kuwada NJ, Craig EM, et al. Realization of a feedback controlled flashing ratchet. Phys Rev Lett. 2008;101:220601.
[28] Admon T, Rahav S, Roichman Y. Experimental realization of an information machine with tunable temporal correlations. Phys Rev Lett. 2018;121:180601.
[29] Ribezzi-Crivellari M, Ritort F. Large work extraction and the Landauer limit in a continuous Maxwell demon. Nat Phys. 2019;15:660.
[30] Koski JV, Maisi VF, Pekola JP, et al. Experimental realization of a Szilard engine with a single electron. Proc Nat Acad Sci. 2014;111:13786.
[31] Vidrighin MD, Dahlsten O, Barbieri M, et al. Photonic Maxwell's Demon. Phys Rev Lett. 2016;116:050401.
[32] Masuyama Y, Funo K, Murashita Y, et al. Information-to-work conversion by Maxwell's demon in a superconducting circuit quantum electrodynamical system. Nat Commun. 2018;9:1291.
[33] Bérut A, Arakelyan A, Petrosyan A, et al. Experimental verification of Landauer's principle linking information and thermodynamics. Nature. 2012;483:187.
[34] Jun Y, Gavrilov M, Bechhoefer J. High-precision test of Landauer's principle in a feedback trap. Phys Rev Lett. 2014;113:190601.
[35] Koski JV, Maisi VF, Sagawa T, et al. Experimental observation of the role of mutual information in the nonequilibrium dynamics of a Maxwell Demon. Phys Rev Lett. 2014;113:030601.
[36] Kwon C, Um J, Park H. Information thermodynamics for a multi-feedback process with time delay. EPL (Europhysics Letters). 2017;117:10011.
[37] Pal PS, Rana S, Saha A, et al. Extracting work from a single heat bath: a case study of a Brownian particle under an external magnetic field in the presence of information. Phys Rev E. 2014;90:022143.
[38] Murashita Y, Funo K, Ueda M. Nonequilibrium equalities in absolutely irreversible processes. Phys Rev E. 2014;90:042110.
[39] Ashida Y, Funo K, Murashita Y, et al. General achievable bound of extractable work under feedback control. Phys Rev E. 2014;90:052125.
[40] Martínez IA, Roldán É, Dinis L, et al. Colloidal heat engines: a review. Soft Matter. 2017;13:22.
[41] Albay JAC, Paneru G, Pak HK, et al. Optical tweezers as a mathematically driven spatio-temporal potential generator. Opt Express. 2018;26:29906.
[42] Sagawa T, Ueda M. Generalized Jarzynski equality under nonequilibrium feedback control. Phys Rev Lett. 2010;104:090602.
[43] Bauer M, Abreu D, Seifert U. Efficiency of a Brownian information machine. J Phys A. 2012;45:162001.
[44] Bialek WS. Biophysics: searching for principles. Princeton, NJ: Princeton University Press; 2012.
[45] Selimkhanov J, Taylor B, Yao J, et al. Accurate information transmission through dynamic biochemical signaling networks. Science. 2014;346:1370.
[46] Barato AC, Hartich D, Seifert U. Efficiency of cellular information processing. New J Phys. 2014;16:103024.
[47] Ito S, Sagawa T. Maxwell's demon in biochemical signal transduction with feedback loop. Nat Commun. 2015;6:7498.

[48] Paneru G, Dutta S, Tlusty T, et al. Approaching and violating thermodynamic uncertainty bounds in measurements of fluctuation-dissipation tradeoffs of information engines. Preprint. 2019.
[49] Li T, Kheifets S, Raizen MG. Millikelvin cooling of an optically trapped microsphere in vacuum. Nat Phys. 2011;7:527.
[50] Martínez IA, Roldán É, Parrondo JMR, et al. Effective heating to several thousand kelvins of an optically trapped sphere in a liquid. Phys Rev E. 2013;87:032159.
[51] Verley G, Esposito M, Willaert T, et al. The unlikely Carnot efficiency. Nat Commun. 2014;5:4721.
[52] Proesmans K, Van de Broeck C. Stochastic efficiency: five case studies. New J Phys. 2015;17:065004.
[53] Verley G, Willaert T, Van den Broeck C, et al. Universal theory of efficiency fluctuations. Phys Rev E. 2014;90:052145.
[54] Park J-M, Chun H-M, Noh JD. Efficiency at maximum power and efficiency fluctuations in a linear Brownian heat-engine model. Phys Rev E. 2016;94:012127.
[55] Manikandan SK, Dabelow L, Eichhorn R, et al. Efficiency fluctuations in microscopic machines. Phys Rev Lett. 2019;122:140601.
[56] Rana S, Pal PS, Saha A, et al. Single-particle stochastic heat engine. Phys Rev E. 2014;90:042146.
[57] Saha A, Marathe R, Pal PS, et al. Stochastic heat engine powered by active dissipation. J Stat Mech. 2018;2018:113203.
[58] Saha A, Marathe R. Stochastic work extraction in a colloidal heat engine in the presence of colored noise. J Stat Mech. 2019;2019:094012.
[59] Polettini M, Verley G, Esposito M. Efficiency statistics at all times: carnot limit at finite power. Phys Rev Lett. 2015;114:050601.
[60] Proesmans K, Dreher Y, Gavrilov M, et al. Brownian duet: a novel tale of thermodynamic efficiency. Phys Rev X. 2016;6:041010.
[61] Proesmans K, Cleuren B, Van den Broeck C. Stochastic efficiency for effusion as a thermal engine. EPL (Europhysics Letters). 2015;109:20004.
[62] Sagawa T, Ueda M. Nonequilibrium thermodynamics of feedback control. Phys Rev E. 2012;85:021104.
[63] Horowitz JM, Esposito M. Thermodynamics with continuous information flow. Phys Rev X. 2014;4:031015.
[64] Barato AC, Seifert U. An autonomous and reversible Maxwell's demon. Epl-Europhys Lett. 2013;101:60001.
[65] Koski JV, Kutvonen A, Khaymovich IM, et al. On-chip Maxwell's Demon as an information-powered refrigerator. Phys Rev Lett. 2015;115:260602.
[66] Serra-Garcia M, Foehr A, Molerón M, et al. Mechanical autonomous stochastic heat engine. Phys Rev Lett. 2016;117:010602.